

Short Communication

Effect of Annealing on Crystal Orientation and Electrochemical Performance of Nanocrystalline LiFePO₄

Wen-Li Kong¹, Yi-Jie Gu^{1,*}, Hong-Quan Liu¹, Yun-Bo Chen², Jie Yang¹, Cheng-Quan Liu³

¹ College of Materials Science and Engineering, Shandong University of Science and Technology, Qingdao 266510, China

² Advanced Manufacture Technology Center, China Academy of Machinery Science and Technology, Beijing 100044, China

³ Henan ZhongPingHanBo New Energy Co., Ltd., Pingdingshan 467000, China

*E-mail: 13792900643@163.com

Received: 14 November 2017 / Accepted: 2 January 2018 / Published: 5 February 2018

Nano single-crystalline LiFePO₄ (LFP) with large (010) plane exposure was synthesized by the hydrothermal method, followed by annealing to alleviate the main limitations of LiFePO₄ cathode material. The XRD results indicated that after annealing, the sample gained the preferred crystal orientation with a (020) crystallographic direction. Annealed LiFePO₄ showed a significantly improved capacity and excellent cycling and rate stability. Further electrochemical impedance analysis indicated that annealed LiFePO₄ has smaller film resistance R_{sf} , smaller charge-transfer resistance R_{ct} , and a larger diffusion coefficient of lithium ion (D_{Li}).

Keywords: LiFePO₄; annealing; crystal orientation; electrochemical impedance

1. INTRODUCTION

Olivine-structured LiFePO₄ has been studied extensively since its introduction as the cathode material for lithium ion batteries by Goodenough, because of its unique properties such as large theoretical capacity (170 mAh g⁻¹), excellent thermal stability, cycling stability, long cycle life, superior safety performance, low cost, and high compatibility to the environment [1-4]. However, its poor electronic conductivity and low lithium-ion diffusion coefficient restrict its extensive application [5, 6]. Several approaches have been proposed to overcome these drawbacks, including size reduction, conductive surface coating, and doping with an alien ion [6-10]. The hydrothermal method has been considered to be a promising method for mass production and large-scale industrial application of LiFePO₄. This method allows economic production of LiFePO₄ with excellent crystallinity, high

purity, high uniformity, desirable morphology and structure, and superior performance at a relatively low temperature [10, 11].

Post-annealing is used to enhance the various properties of LiFePO_4 cathode material, such as capacity, cycling stability, and rate capability owing to enhanced crystallization, conductivity, and lesser defects [12-14]. However, LiFePO_4 powders sintered at low temperatures (≤ 500 °C) exhibit unsatisfactory performance because of lower utilization caused by a lower level of crystallinity and unsettled defects [15-17]. At the same time, abnormal growth occurs at annealing temperatures above 700 °C because of the fusion of LiFePO_4 into larger particles, which deteriorate the electrochemical performance [15, 18]. Since 600 °C is the suitable temperature for post-annealing, changes in the crystal structure, particle size, morphology, and electrochemical performance of LiFePO_4 powders annealed at 600 °C for 5h are investigated in this study.

2. EXPERIMENTAL

Pristine LiFePO_4 was synthesized by the hydrothermal method using $\text{LiOH}\cdot\text{H}_2\text{O}$, $\text{FeSO}_4\cdot 7\text{H}_2\text{O}$, and H_3PO_4 with a molar ratio of 3:1:1 in an aqueous solution. Firstly, $\text{LiOH}\cdot\text{H}_2\text{O}$ and $\text{FeSO}_4\cdot 7\text{H}_2\text{O}$ were dissolved separately in deionized water, and ascorbic acid was introduced into the FeSO_4 solution as a reducing agent. H_3PO_4 was then cautiously added dropwise into a vigorously agitated LiOH solution with IPA, followed by slow addition of the aqueous solution of FeSO_4 into the resulting white suspension of Li_3PO_4 . A blue mixture was eventually obtained, and the pH of the slurry was adjusted by adding H_3PO_4 . The resulting suspension was then quickly transferred into a 100 mL Teflon-lined stainless steel autoclave. The reactor was heated at 200 °C for 12h. After cooling down, the precipitate was centrifuged and washed several times with deionized water, and the obtained gray filter cake was vacuum-dried at 120 °C for 12h. The ferrous iron (Fe^{2+}) content was determined titrimetrically using potassium dichromate standard solution. The phosphorus content (PO_4^{3-}) was determined gravimetrically using the quinoline phosphomolybdate gravimetric method. The Fe/P ratio is 1, and the Fe and P content of the sample are 34.575 and 19.155 % wt. The LiFePO_4 powder was then annealed at 600 °C for 5 h under a N_2 atmosphere.

The crystallographic structures of the products were determined by powder X-ray diffraction (XRD, D/Max2500PC, Japan) with $\text{Cu-K}\alpha$ radiation, a graphite monochromator, a tube voltage of 30 kV, a tube current of 100 mA, and a step size of 0.02° from 10° to 120° . The particle size and morphology of the powders were characterized by field emission scanning electron microscopy (FESEM, Nova Nano SEM450, USA) and transmission electron microscopy (TEM, JEM2100F, Japan), respectively. The particle size and distribution were analyzed by Nano Measure software. The cathodes were by mixing the active materials with carbon black and polyvinylidene fluoride (PVDF) in a weight ratio of 85:9:6 in N-methyl-2-pyrrolidone to form slurry. The resultant mixtures were pasted onto Al foils, dried at 120 °C for 12 h in a vacuum oven, and then punched into circular disks using a roll-press machine. Test cells with a coin-type cell (size: CR2016) were assembled in a high-purity argon-filled glove box in a two-electrode configuration using the cathode composite, lithium metal as the anode, and Celgard 2400 as the separator. The electrolyte comprised 1 M LiPF_6 solution in ethylene

carbonate:dimethyl carbonate:ethyl methyl carbonate with a 1:1:1 volume ratio. Galvanostatic charge/discharge tests were performed over a voltage range of 2–4 V with a battery test system (LAND-CT2001A, China). Electrochemical impedance spectroscopy was performed using an impedance analyzer (Zahner Elektrik IM6, Germany) over a frequency range of 100 mHz–100 kHz with an amplitude of 5 mV.

3. RESULTS AND DISCUSSION

Fig. 1 shows the X-ray diffraction patterns of pristine LiFePO_4 before and after annealing. All the samples are single-phase LiFePO_4 with an olivine structure, which are indexed to an orthorhombic space group Pnma (JCPDS Card No: 83-2092); no impurities are detected. The diffraction peaks of samples are well split and have strong intensity. All samples have high purity and show considerably good crystallization. The X-ray diffraction pattern of the LiFePO_4 sample after annealing was further refined by a Rietveld method and is shown in Fig. 2. The cell parameters obtained from Rietveld refinement are: $a=10.32642(13)$ Å, $b=6.00482(8)$ Å, $c=4.69095(7)$ Å consistent with standard values of JCPDS Card No: 83-2092. Compared with the pristine unannealed LiFePO_4 , the intensity of the diffraction peaks increased after annealing due to improved crystallinity and reduced defects. The diffraction peak intensity of (020) and (111) of LiFePO_4 undergo subtle changes after annealing. The diffraction peak intensity of (020) (denoted as $I_{(020)}$) is weaker than that of (111) (denoted as $I_{(111)}$) before annealing.

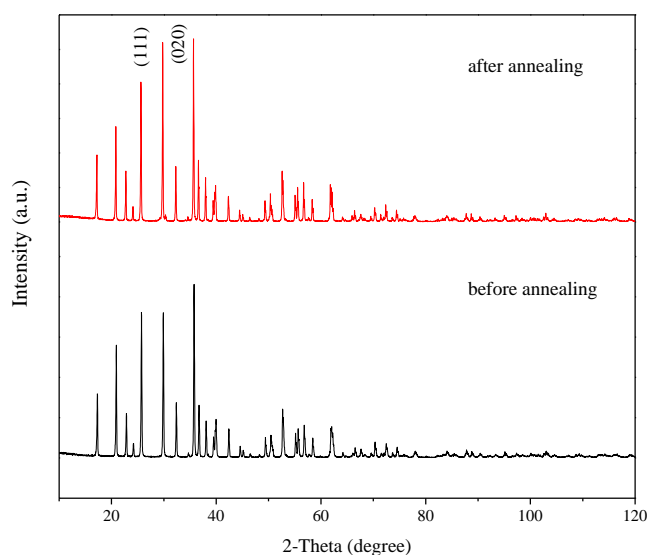


Figure 1. XRD pattern of pristine LiFePO_4 before and after annealing.

There was a significant increase in the diffraction peak intensity of (020) after annealing, and $I_{(020)}$ is higher than $I_{(111)}$, indicating that after annealing, the sample had some preferred crystal orientation with a (020) crystallographic direction. In order to compare the diffraction peak intensity of (020) and (111), the ratios of $I_{(020)}/I_{(111)}$ for two samples are listed in Table 1. The peak intensity ratio

of $I_{(020)}/I_{(111)}$ for pristine unannealed LiFePO_4 is 0.9816, while the ratio after annealing is 1.2854. The intensity of the (020) diffraction peak increased after annealing because the (010) plane is prominent, as shown by both calculated and experimentally determined morphologies, and the energy of the (010) surface is the lowest among the 19 low index planes of LFP, as pointed out by Islam's group [19]. Thus, it can be said that the post-heat treatment exerts a significant influence on the growth orientation and (010) crystallographic direction of LiFePO_4 .

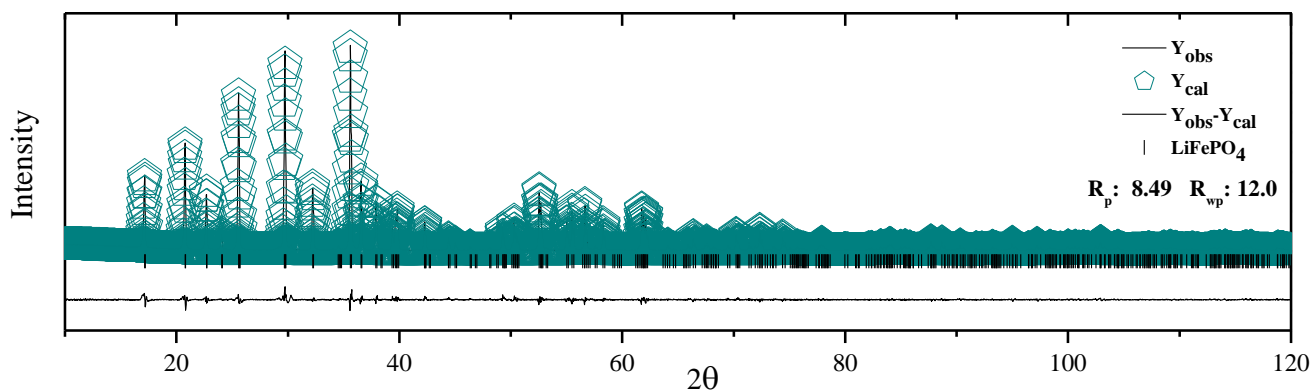


Figure 2. Rietveld refinement of pristine LiFePO_4 after annealing.

Table 1. The ratios of peak intensity of (020) and (111) plane about pristine LiFePO_4 before and after annealing.

Sample	$I_{(020)}/I_{(111)}$
before annealing	0.9986
after annealing	1.2852

The SEM microphotographs of pristine LiFePO_4 before and after annealing are shown in Fig. 3. The samples' morphologies remain almost constant, and all the particles are highly crystallized, neat, and well mono-dispersed. Both samples present tiny cuboid-like shapes and elongated rod shapes, and show large {010} faces. Particle size is measured by Nano Measure software, and a wide size distribution is obtained (ranging from 100 nm to 1.3 μm long; Fig. 4). The excellent grain size distribution can lead to high tap density, which enhances the electrochemical performance of cathode materials. The post-heat treatment process had no effect on the particle morphology, but showed a slight effect on the grain size of LiFePO_4 . The particle size distribution shifted to a smaller size, and the crystals shortened in length, width and thickness owing to enhanced crystallinity and reduced defects.

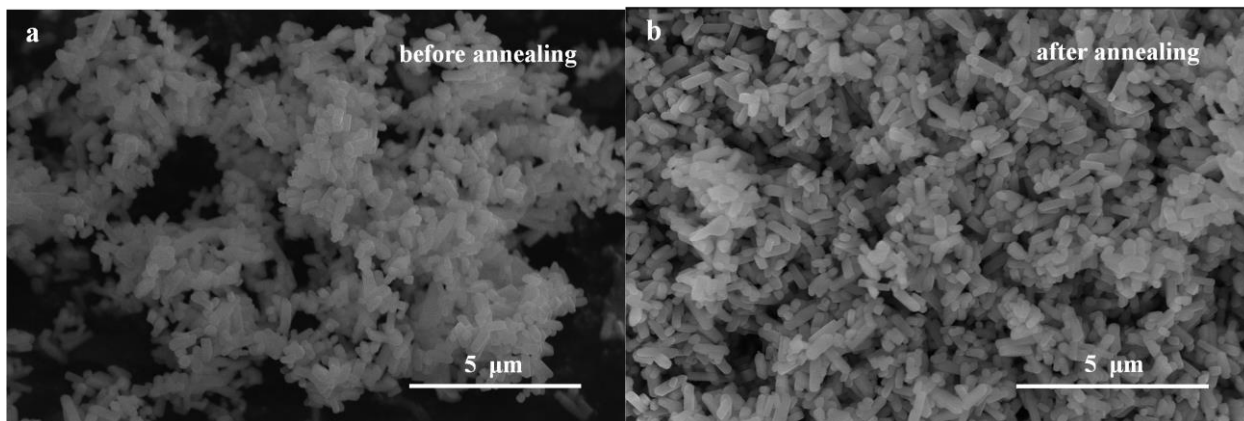


Figure 3. SEM images of pristine LiFePO₄ before and after annealing.

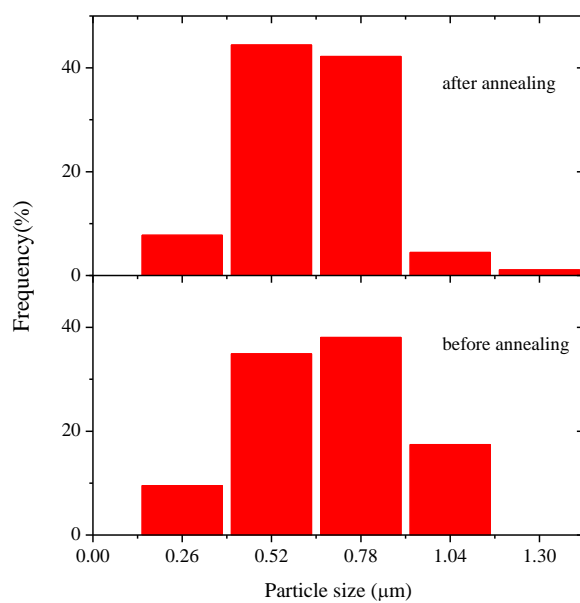
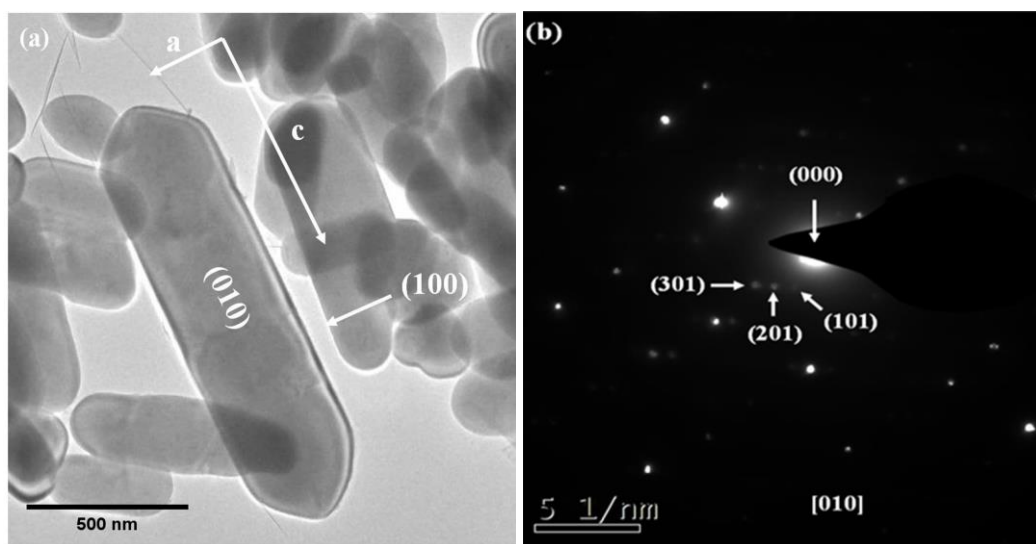


Figure 4. Comparison of particle size distribution of pristine LiFePO₄ before and after annealing.



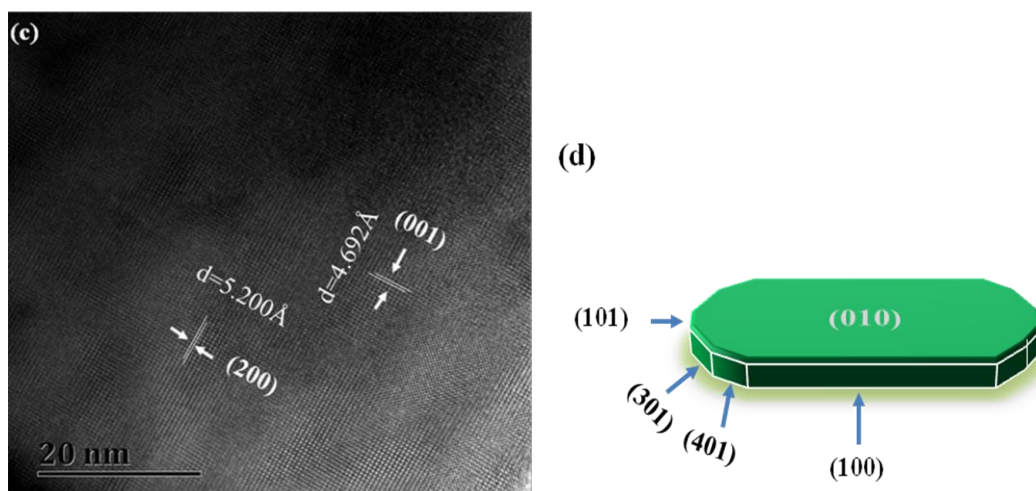


Figure 5. TEM image and the selected area electron diffraction (SAED) pattern of pristine LiFePO_4 after annealing (a,b). LiFePO_4 hexagonal nanorods have predominant (010) face exposure, and the side of nanorods is (100) plane. HRTEM and simulated morphology of LiFePO_4 crystal (c,d).

To further study the microstructure of samples, TEM and HRTEM analyses were conducted. As shown in the TEM image (Fig. 5(a)), the particles exhibit morphology in which (010) and (100) are prominent and (010) faces are predominantly exposed, in accordance with the results reported in literature [20-22]. The formation mechanism and dominant growth habit exhibits the {020}, {200} and {101} faces under hydrothermal conditions in a weak acidic solution were investigated by calculating the stability energy of the crystal growth unit, surface structures, and molecular simulation [23]. The predominantly exposed face on the (010) plane can be confirmed based on the selected area electron diffraction (SAED) pattern shown in Fig. 5(b).

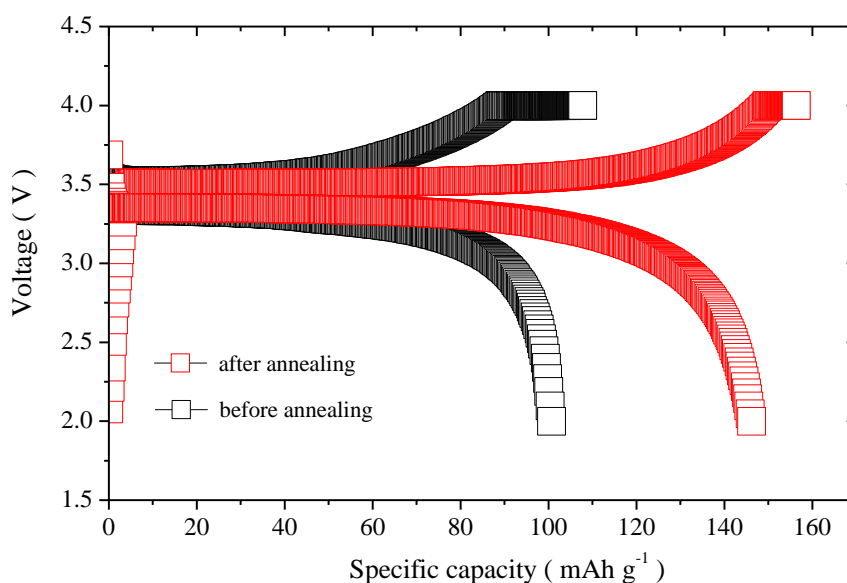
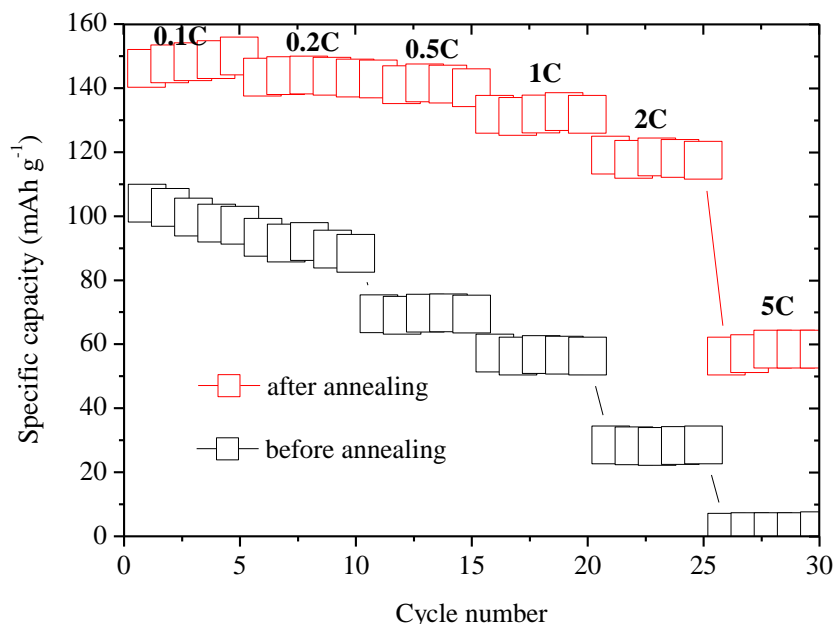


Figure 6. Comparison of initial charge-discharge curves of pristine LiFePO_4 before and after annealing at 0.1C.

Table 2. Initial charge/discharge capacities and coulomb efficiency of pristine LiFePO₄ before and after annealing.

sample	Charge capacity (mAh g ⁻¹)	discharge capacity (mAh g ⁻¹)	Efficiency (%)
before annealing	107.8	100.7	93.3
after annealing	156.4	146.2	93.4

**Figure 7.** Cycle and Rate performance of pristine LiFePO₄ before and after annealing.

The sample exhibits regular lattice fringes of the (200) crystalline plane with a measured d spacing value of 5.200 Å, and the (001) crystalline plane with a measured d spacing of 4.692 Å. The simulated morphology of the LiFePO₄ crystal is shown in Fig. 5(d), and the top of nanorod consists of (101), (301), and (401) planes. The crystal orientation of LiFePO₄ in the (010) crystallographic direction exerts significant effect on the charge-discharge process because of the migration of Li along the [010] channel, as the charge transfer takes place mainly in the favorable (010) crystallographic direction [21, 23].

The constant-current charge/discharge curves of samples for the first cycle, at a current rate of 0.1C, are shown in Fig. 6. Poor initial cycle charge/discharge capacities of unannealed LiFePO₄ are 107.8 and 100.7 mAh g⁻¹, respectively. The annealed sample displays a significant enhancement of the electrochemical performance and shows charge and discharge capacities of 156.4 and 146.2 mAh g⁻¹ at 0.1C, respectively. And discharge capacity of annealed LiFePO₄ reaches to 143.4 mAh g⁻¹ at 0.2C. In the absence of a secondary carbon source, the discharge capacities of LiFePO₄ powder are 113 and 137 mAh g⁻¹ at 0.2C, respectively.[24,25] The initial specific charge capacity, discharge capacity, and coulomb efficiency of the samples are listed in Table. 2. The C-rate capability and cycling performance of samples at 0.1C, 0.2C, 0.5C, 1C, 2C and 5C rates are shown in Fig. 7. The pristine unannealed LiFePO₄ shows significant capacity fading with increasing current density, because poor kinetics of Li⁺

diffusion and electron transfer can not sustain fast charge and discharge. A significant improvement in the C-rate capability and cycling performance can be observed after post-heat treatment. LiFePO_4 powders after annealing show higher capacity and much slower capacity decay than those of unannealed LiFePO_4 . When the C rate increases, the interval of discharge capacities between two cathodes becomes larger, which indicates that the annealed sample has lower electrochemical resistance and excellent reversible reaction kinetics during the cycles.

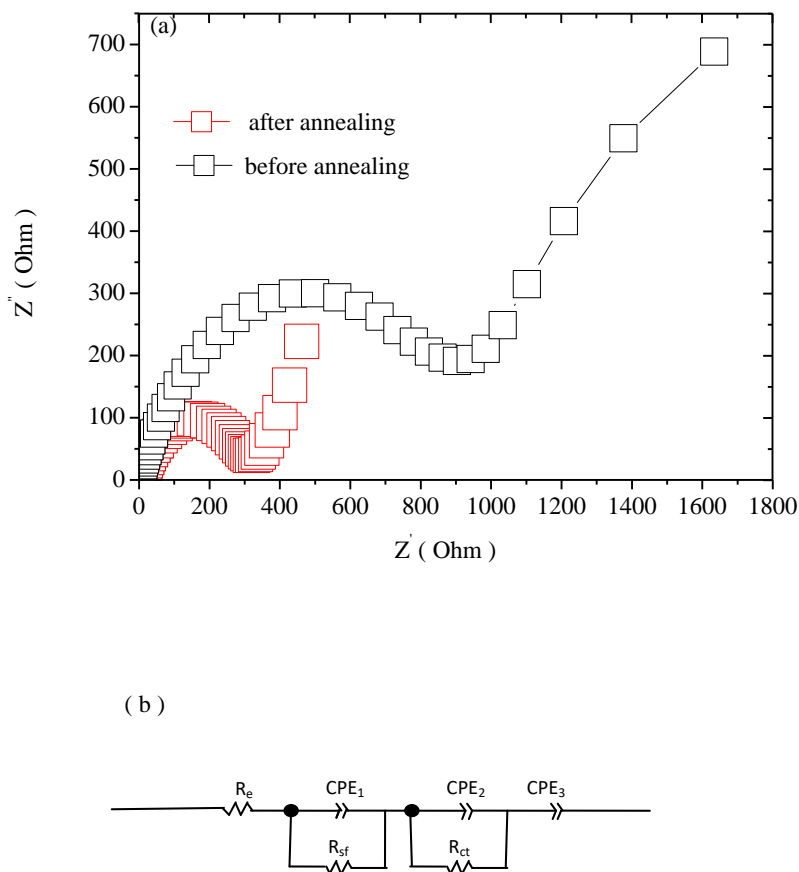


Figure 8. Impedance spectra of pristine LiFePO_4 before and after annealing : (a) Nyquist plots; (b) equivalent circuit model. The frequency range and pulse amplitude applied were 100 kHz-100 mHz and 5 mV, respectively.

To further analyze the electron transfer process of the samples, electrochemical impedance spectroscopy (EIS) was carried out. The corresponding Nyquist plots of the spectra and the selected equivalent circuit are shown in Fig. 8. Both the impedance spectra have an arc in the high-frequency region, a semicircle in the middle-frequency region, and a linear spike in the low-frequency region. The intercept on the Z_{real} axis in the high-frequency region corresponds to the ohmic resistance R_s , which includes electrolyte solution resistance and electric contact resistance. The arc in the high-

frequency region is related to R_{sf} (the resistance of lithium ion diffusion through the solid electrolyte interface (SEI) resulted from the reaction between the electrolyte and the electrode on the electrolyte-electrode interface). The semicircle in the middle-frequency region involves the charge-transfer resistance R_{ct} between Li^+ ion and electron, and the straight line in the low-frequency region corresponds to the Warburg impedance, which is related to lithium-ion diffusion in the bulk.

To further investigate the electrochemical impedance of the samples, the simulation results of R_{sf} and R_{ct} using the established equivalent circuit are listed and compared in Table 3. The pristine unannealed $LiFePO_4$ has larger R_{sf} and R_{ct} values of 44.35 and 578.9 Ω , respectively, due to low crystallization grade, defects, and inherently sluggish kinetics of Li^+ ion and electron migration. The calculated diffusion coefficient of lithium ion (D_{Li^+}) of $LiFePO_4$ without annealing is $1.6082 \times 10^{-16} \text{ cm}^2 \text{ s}^{-1}$. The annealed $LiFePO_4$ has lower electrochemical resistance, with the R_{sf} and R_{ct} values of 25.22 and 223.4 Ω , respectively. The diffusion coefficient of lithium ion (D_{Li^+}) of annealed $LiFePO_4$ increases to $5.8585 \times 10^{-15} \text{ cm}^2 \text{ s}^{-1}$, indicating that annealing enhances the mobility of lithium ion and electron, resulting in better electrochemical performance.

Table 3. Result of the electrochemical impedance for pristine $LiFePO_4$ before and after annealing.

sample	$R_{sf}(\Omega)$	$R_{ct}(\Omega)$	$\sigma (\text{s cm}^{-2})$	$D(\text{cm}^2 \text{ s}^{-1})$
before annealing	44.35	578.9	679.19734	1.6082×10^{-16}
after annealing	25.22	223.4	112.5313	5.8585×10^{-15}

4. CONCLUSION

Post-annealing is performed to enhance the performance of $LiFePO_4$ nanorods prepared by the hydrothermal method. The significant improvement in the capacity, cycling stability, and rate capability is understood based on the control of both crystal orientation and electrochemical impedance. The structure of $LiFePO_4$ has changed after annealing, in addition to increased crystallinity, there are crystal orientation with a (020) crystallographic direction. Film resistance R_{sf} and charge-transfer resistance R_{ct} reduced by half after annealing, while the diffusion coefficient of lithium ion (D_{Li}) increased by an order of magnitude over that of unannealed $LiFePO_4$. The results of this study have practical significance for the synthesis and preparation of lithium iron phosphate for improving the electrochemical performance of cathode materials.

ACKNOWLEDGEMENTS

This work was financially supported by the National Natural Science Foundation of China (No. 51641206), Postdoctoral Science Foundation of China (2013M541907), and Special funds for Independent Innovation and Transformation of Achievements in Shandong Province (Grant No. 2014CGZH0911).

References

1. A.K. Padhi, K.S. Nanjundaswamy, J.B. Goodenough, *J. Electrochem. Soc.*, 144 (1997) 1188.
2. S. Ferrari, R.L. Lavall, D. Capsoni, E. Quartarone, A. Magistris, P. Mustarelli, P. Canton, *J. Phys. Chem. C*, 114 (2010) 12598.
3. M.K. Devaraju, I. Honma, *Adv. Energy Mater.*, 2 (2012) 284.
4. Y. Zhao, L. Peng, B. Liu, G. Yu, *Nano Lett.*, 14 (2014) 2849.
5. J.J. Wang, X.L. Sun, *Energy Environ. Sci.*, 5 (2012) 5163–5185.
6. B. Wang, B. Xu, T. Liu, P. Liu, C. Guo, S. Wang, Q. Wang, Z. Xiong, D. Wang, X. S. Zhao, *Nanoscale*, 6 (2014) 986.
7. K. Saravanan, P. Balaya, M.V. Reddy, B.V.R. Chowdari, J.J. Vittal, *Energy Environ. Sci.*, 3 (2010) 457.
8. B. Kang, G. Ceder, *Nature*, 458 (2009) 190.
9. J. Yang, J. Wang, Y. Tang, D. Wang, X. Li, Y. Hu, R. Li, G. Ling, T. –K. Sham, X. Sun, *Energy Environ. Sci.*, 6 (2013) 1521.
10. S.Y. Chung, J.T. Bloking, Y.M. Chiang, *Nat. Mater.*, 1 (2002) 123.
11. K. DoKKo, S. Koizumi, K. Sharaishi, K. Kanamura, *J. Power Sources*, 165 (2007) 659.
12. O. Waser, R. Büchel, A. Hintennach, P. Novák, S.E. Pratsinis, *J. Aerosol Sci.*, 42 (2011) 657.
13. Y-N. Xu, S-Y. Chung, J.T. Blocking, Y-M. Chiang, W.Y. Ching, *Electrochem. Solid-State Lett.*, 7 (2004) 881.
14. R. Amin, J. Maier, *Solid State Ionics*, 178 (2008) 1831.
15. F. Gao, Z. Y. Tang, J.J. Xue, *Electrochim. Acta*, 53 (2008) 1939.
16. J. Chen, J. Graetz, *ACS Appl. Mater.*, 3 (2011) 1380.
17. S. Yang, Y. Song, P.Y. Zavalij, M.S. Whittingham, *Electrochem. Commun.*, 4 (2002) 239.
18. F. Krumeich, O. Waser, S.E. Pratsinis, *J. Solid State Chem.*, 242 (2016) 96.
19. C.A.J. Fisher, M.S. Islam, *J. Mater. Chem.*, 18 (2008) 1209.
20. K. Kanamura, S. Koizumi, *J. Mater. Sci.*, 43 (2008) 2138.
21. B.L. Ellis, K.T. Lee, L.F. Nazar, *Chem. Mater.*, 22 (2010) 691–714.
22. G. Chen, X. Song, T.J. Richardson, *Electrochem. Solid-State Lett.*, 9 (2006) : A295.
23. C.H. Xu, L. Wang, X.G. He, J.L. Y.M. Shang, J.L. Wang, *Int. J. Electrochem. Sci.*, 11 (2016) 1558.
24. Y. Ding, Y. Jiang, F. Xu, J. Yin, H. Ren, Q. Zhou, Z. Long, P. Zhang, *Electrochem Commun.*, 12 (2010) 10.
25. Y.D. Cho, G.T.K. Fey, H.M. Kao, *J. Power Sources*, 189 (2009) 256.